JOURNAL OF GUIDANCE, CONTROL, AND DYNAMICS
Vol. 32, No. 6, November–December 2009

Comparison of the Radar and Seeker Modes of Pursuer Guidance

A. K. Sarkar*
Defence Research and Development Laboratory, Hyderabad 500 058, India
M. R. Ananthasayanam†
Indian Institute of Science, Bangalore 560 012, India
and
T. Srinivasan‡ and P. K. Kar‡
Defence Research and Development Laboratory, Hyderabad 500 058, India

DOI: 10.2514/1.40404

This paper compares closed-loop performance of seeker-based and radar-based estimators for surface-to-air interception through 6-degree-of-freedom simulation using proportional navigation guidance. Ground radar measurements are evader range, azimuth and elevation angles contaminated by Gaussian noise. Onboard seeker measurements are pursuer–evader relative range, range rate also contaminated by Gaussian noise. The gimbal angles and line-of-sight rates in the gimbal frame, contaminated by time-correlated non-Gaussian noise with realistic numerical values are also available as measurements. In both the applications, extended Kalman filter with Gaussian noise assumption are used for state estimation. For a typical engagement, it is found that, based on Monte Carlo studies, seeker estimator outperforms radar estimator in terms of autopilot demand and reduces the miss distance. Thus, a seeker estimator with white Gaussian assumption is found to be adequate to handle the measurements even in the presence of non-Gaussian correlated noise. This paper uses realistic numerical values of all noise parameters.

Nomenclature

(a_{mx}, a_{my}, a_{mz})	=	pursuer inertial acceleration components
(a_{tx}, a_{ty}, a_{tz})	=	evader inertial acceleration components
(K_{sl}, K_v)	=	seeker servo, track-loop gain
$(\mathbf{P}, \mathbf{P_0})$	=	system and initial state covariance
(p, q, r)	=	body rates along body frame of pursuer
$\mathbf{R}_c$	=	radar Cartesian noise covariance
$\mathbf{R}_p$	=	radar polar noise covariance
$(r, \dot{r})$	=	range, range rate (pursuer–evader relative)
$(r_l, \dot{r}_l)$	=	relative range, range rate along line of sight
(r_m, a_m, e_m)	=	measured range, azimuth, elevation
(r_t, a_t, e_t)	=	true range, azimuth, elevation
T_s	=	radar estimator sampling time
(V_c, V_m, V_t)	=	closing, pursuer, evader velocity
(V_{mx}, V_{my}, V_{mz})	=	pursuer velocity, inertial
(V_{tx}, V_{ty}, V_{tz})	=	evader velocity, inertial
(V_{xe}, V_{yn}, V_{zu})	=	pursuer velocity (east, north, up)
$(w_{a_{tx}}, w_{a_{ty}}, w_{a_{tz}})$	=	Gaussian acceleration process noise
$(\mathbf{X}, \mathbf{X}_0)$	=	system and initial state vector
(x_m, y_m, x_m)	=	pursuer inertial position components
(x_t, y_t, y_t)	=	evader inertial position components
$(\Delta V_x, \Delta V_y, \Delta V_z)$	=	pursuer, evader relative inertial velocity
$(\Delta x, \Delta y, \Delta z)$	=	pursuer, evader relative inertial position
$(\varepsilon_y, \varepsilon_p)$	=	gimbal angle tracking error (yaw, pitch)
(η_y, η_p)	=	demanded latax (yaw, pitch)
(μ, σ)	=	mean and standard deviation
ν_k	=	innovation during the kth measurement
(ν_1, ν_2, ν_3)	=	radar measurement noise in Cartesian frame
$(\sigma_{ax}, \sigma_{ay}, \sigma_{az})$	=	target acceleration uncertainty, Cartesian frame
$(\sigma_{\phi_g}, \sigma_{\gamma_g})$	=	random noise of gimbal angles, one σ
(τ_x, τ_y, τ_z)	=	target acceleration time constant lag
(ϕ_g, γ_g)	=	gimbal angles along inner gimbal frame
(ϕ_l, γ_l)	=	evader line-of-sight angles (line-of-sight frame)
(ϕ_m, γ_m)	=	pursuer gimbal angles (inner gimbal frame)
(ϕ_t, γ_t)	=	evader yaw and pitch angle (inertial frame)
$(\phi_l, \dot{\gamma}_l)$	=	evader line-of-sight rate (line-of-sight frame)
$(\omega_1, \ldots, \omega_9)$	=	process noise components in radar estimator
$(\omega_{gz}, \omega_{gy})$	=	line-of-sight rate of evader along inner gimbal frame

Presented as Paper 7462 at the AIAA Guidance, Navigation, and Control Conference and Exhibit, Honolulu, HI, 18–21 August 2008; received 14 August 2008; revision received 10 August 2009; accepted for publication 3 May 2009.

*Scientist, Directorate of Systems, Kanchanbagh; a_krishna_sarkar@yahoo.com.
†Former Professor, Aerospace Engineering Department; sayanam2005@yahoo.co.in.
‡Scientist, Directorate of Systems, Kanchanbagh.

Introduction

IN AN air combat scenario, the pursuer–evader guidance problem is generally solved by the proportional navigation (PN) principle. In real-world radar-based guidance, evader range, azimuth and elevation angles as measurements are assumed to be contaminated by Gaussian white noise. They are processed to estimate evader position and velocity by an extended Kalman filter (EKF) based state estimator and are uplinked to the pursuer to generate onboard guidance commands [1]. Similarly, in real-world seeker-based guidance, the pursuer onboard active radio frequency seeker measures pursuer–evader relative range, and range rate contaminated by assumed Gaussian white noise. The gimbal angles and relative line-of-sight (LOS) rates in the inner gimbal (IG) frame are also available as measurements contaminated by non-Gaussian colored noise. Further, LOS rate noise is high due to glint, radar cross section (RCS) fluctuation, and thermal effects. Corresponding signal-to-noise ratio (SNR) in LOS rates vary from a low value of 3 dB to a high value of 50 dB. This is a function of range to go from evader lock on until interception. Also, in a seeker with a single high pulse repetition frequency, signal loss occurs due to eclipsing. This results in intermittent data loss in LOS rate measurements. Under these conditions, the seeker estimator has to estimate pursuer–evader relative state

variables for guidance command generation. Previous researchers have carried out studies on the seeker estimator assuming the available measurements in the LOS frame. Conceptually, this is correct, but in actual seeker hardware all the measurements are in the seeker IG frame. The relative range and range rate equations are similar to that of radar. The gimbal angles, the angular movements of gimbals, and relative LOS rates along pitch and yaw planes are generated in the IG frame from the tracking error of the gimbal angles in the presence of body rate coupling. These measurements being in the gimbal frame, certain orthogonal transformations from true LOS frame to gimbal frame are required (Figs. 1 and 2). The kinematic state and measurement equations also consist of pursuer acceleration components and attitude quaternions as input. These features make seeker estimator design more involved than that of radar.

Recently, Ananthasayanam et al. [2,3] developed state and measurement equations, respectively, of the seeker estimator in the Cartesian (C) and polar (P) frame (CP), polar and polar frame of the LOS frame, along with polar and polar frame of the seeker IG (PPG) frame as a continuation of Ekstrand's [4] work, and also performed a literature survey on seeker estimator design. Ananthasayanam et al. [2,3] have mechanized both EKF and unscented Kalman filter (UKF) based state estimators with Gaussian noise assumption in an open loop to process the preceding hardware-driven realistic measurements for air-to-air and air-defense applications and also carried out a

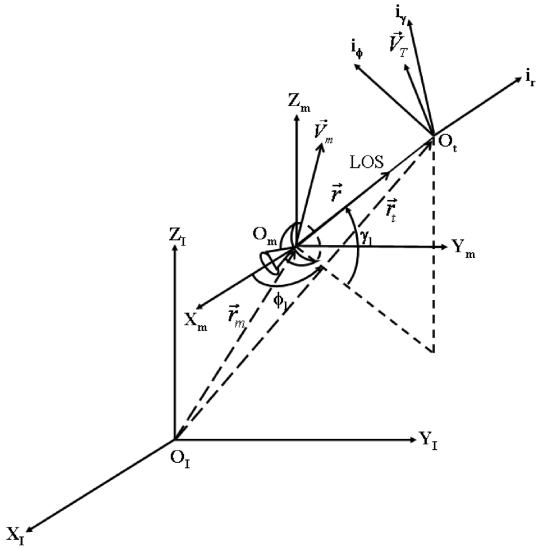

Fig. 1 Axes system for seeker estimator.

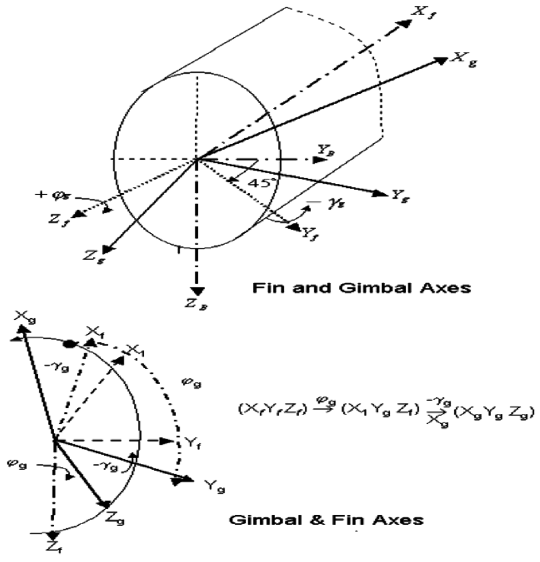

Fig. 2 Axes system for seeker IG frame.

Monte Carlo (MC) based consistency check of estimated states from both EKF and UKF mechanizations based on the preceding formulations. This investigation revealed that, for real world application, the seeker estimators designed with Gaussian noise assumption are, at present, adequate enough to handle non-Gaussian and correlated gimbal angles and LOS rates measurement noise. It turns out to be possible that, by proper filter tuning, estimates through EKF could be obtained within acceptable accuracy. It was also found that filter tuning based on engineering judgment was easiest in the CP frame. Present research is focused on analysis of the seeker-based EKF estimator in the CP frame and comparison of its performance with respect to the corresponding radar estimator for surface-to-air application. This analysis has been carried out by integrating both radar and seeker estimators in a closed loop through realistic 6-degree-of-freedom (6-DOF) simulation for intercepting a maneuvering evader in the presence of the estimator and autopilot lag, actuator, and aerodynamic nonlinearity. The estimated states are used by true proportional navigation (TPN) guidance law to generate pursuer pitch and yaw guidance demands. Zarchan [5] has reported that radar-based command guidance systems have to contend with more noise than seeker-based homing systems, based on a kinematic planar model assuming Gaussian sensor noise. Very recently, Chen et al. [6] proposed two new algorithms for homing guidance and estimation under agile target acceleration. Vaddi et al. [7] have studied pursuer–evader engagement based on pursuer onboard seeker measurements of LOS angles, LOS rates, relative range, and range rate using a 3-DOF simulation model and have reported a miss distance of 0.03 m while intercepting a spiraling evader. Both these studies assumed the LOS angles and rates measurements to be contaminated by Gaussian noise, which is far from reality and not considered 6-DOF simulation analysis in the presence of subsystem lags and estimation error. To the best of our knowledge, such hardware-driven seeker estimator design in the presence of such noisy LOS rates along with eclipsing effect and its performance with respect to the radar estimator design through realistic 6-DOF simulation has not yet been reported in open literature. We have tried to bridge this gap by reporting our 1) realistic hardware-driven kinematic state and measurement equations in the seeker IG frame, 2) synthesis of Gaussian EKF-based seeker estimator for handling gimbal angles and LOS rate measurements contaminated by a high degree of non-Gaussian noise, 3) compatible hardware-driven track-loop formulation and noise model, 4) real-time pursuer onboard computer (OBC) implementable TPN guidance algorithm, and 5) comparative performance study of both the real-world estimators in a typical engagement.

The paper is organized as follows. First, a typical engagement selection from a pursuer flight performance envelope is discussed. Later, EKF-based radar and seeker estimators for a present real-world model are described. Subsequently, comparative performance of radar- and seeker-based guidance based on 6-DOF simulation corresponding to the present engagement with a maneuvering evader is brought out. The evader model, seeker track loop, along with generation of real-world measurements and OBC implementable TPN guidance laws are given in the Appendix. Further simulations show the conclusions to be true for other similar engagements.

Engagement Selection

Generally, a pursuer–evader engagement condition is selected based on the generated flight performance envelope for selecting the initial engagement condition (position, velocity) and maneuver profile of the evader with maximum kill probability. For this purpose, the envelope has been generated under ideal noise-free conditions using a pursuer flyout model [8] consisting of a 6-DOF simulation model of different engagement conditions using aerodynamic database, propulsion, guidance, control, actuation system, and evader kinematic model. The engagement simulations terminate with the negative closing velocity $\mathbf{V}_c$ and miss distance ≤ 10 m. Based on the flight performance envelope, a typical engagement has been chosen as a benchmark for performance study of present radar and seeker estimators. Here, the evader initially is at (8, 0, 6) km from the

pursuer, approaching at speed of 300 m/s at constant altitude. Later, it initiates a $(-3, -3)$ g turn toward the pursuer with a range to go less than 5 km before interception. This turn toward the pursuer is most advantageous to the evader as it forces it to make a tighter turn and expend more energy to keep up with the evader than a turnaway [9]. The pursuer is launched from the ground with (55 deg) elevation, initially with attitude hold autopilot for 2 s. Also during this period, the estimated states of the EKF estimator are allowed to stabilize from initial transients. Then, the TPN guidance law with a navigation constant of four is used until interception. Lateral acceleration (latax) commands generated by guidance are tracked by autopilot along both pitch and yaw planes. Figures 3 and 4 show the schematic diagram of the pursuer–evader engagement in a 6-DOF simulation environment for radar- and seeker-based guidance.

Extended-Kalman-Filter-Based Radar Estimator

The radar measures the true evader position in the P frame as (range, azimuth, elevation) (r, a, e) contaminated by Gaussian noise (η_r, η_a, η_e) with realistic covariance $\mathbf{R}_p$ ($1E04$ m^2, $4E-2$ deg^2, $4E-2$ deg^2). The measurements in P and C frames are related as

$$r_m = \sqrt{x_t^2 + y_t^2 + z_t^2} + \eta_r; \qquad a_m = \tan^{-1}\frac{y_t}{x_t} + \eta_a$$
$$e_m = \tan^{-1}\frac{z_t}{\sqrt{x_t^2 + y_t^2}} + \eta_e \qquad x_{tm} = r_m \cos e_m \cos a_m$$
$$y_{tm} = r_m \cos e_m \sin a_m \qquad z_{tm} = r_m \sin a_m \tag{1}$$

and in the C frame, the state equations are

$$\dot{x}_1 = x_2 + \omega_1; \qquad \dot{x}_2 = x_3 + \omega_2; \qquad \dot{x}_3 = \omega_3$$
$$\dot{y}_1 = y_2 + \omega_4; \qquad \dot{y}_2 = y_3 + \omega_5; \qquad \dot{y}_3 = \omega_6 \tag{2a}$$
$$\dot{z}_1 = z_2 + \omega_7; \qquad \dot{z}_2 = z_3 + \omega_8; \qquad \dot{z}_3 = \omega_9$$

and the measurement equations are

$$x_{tm} = x_1 + \nu_1; \qquad y_{tm} = y_1 + \nu_2; \qquad z_{tm} = z_1 + \nu_3 \tag{2b}$$

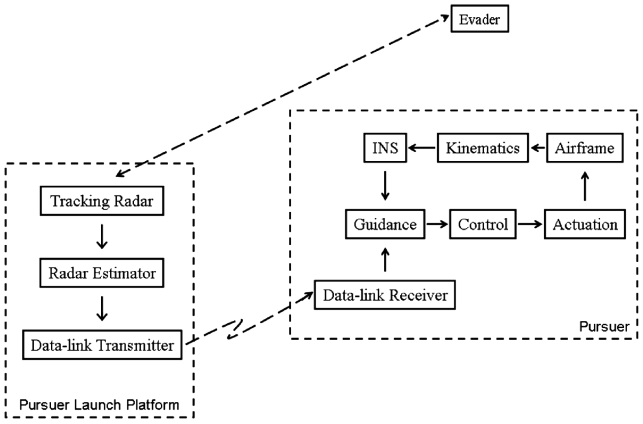

Fig. 3 Radar-based guidance (schematic).

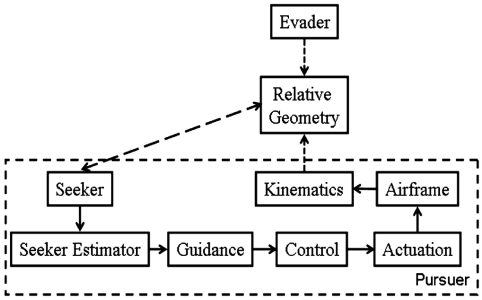

Fig. 4 Seeker-based guidance (schematic).

where $(\omega_1, \ldots, \omega_9)$ and (ν_1, ν_2, ν_3) are, respectively, zero mean process noise and correlated measurement noise with covariance $\mathbf{R}_c$, where $\mathbf{R}_c = \mathbf{J}\mathbf{R}_p\mathbf{J}^T$ and $\mathbf{J}$ is given as [1]

$$\begin{bmatrix} \cos a_m \cos e_m & -r_m \sin a_m \cos e_m & -r_m \cos a_m \sin e_m \\ \sin a_m \cos e_m & r_m \cos a_m \cos e_m & -r_m \sin a_m \sin e_m \\ \sin e_m & 0 & r_m \cos e_m \end{bmatrix}$$

Also, for sampling time T_s, process noise covariance $\mathbf{Q}$ based on Bar-Shalom and Li [10] is given by

$$(Q_x, Q_y, Q_z) = \begin{bmatrix} \frac{T_s^5}{20} & \frac{T_s^4}{8} & \frac{T_s^3}{6} \\ \frac{T_s^4}{8} & \frac{T_s^4}{4} & \frac{T_s^3}{2} \\ \frac{T_s^3}{2} & \frac{T_s^3}{2} & T_s^2 \end{bmatrix} (\sigma_{ax}^2, \sigma_{ax}^2, \sigma_{ax}^2) \tag{3}$$

In the present simulation study, $T_s = 100$ ms, $\sigma_a^2 = 100$, and $\mathbf{P}_0 = 1E08 \times I$ are based on filter tuning experience and engineering judgment. The EKF initialization is based on Singer's method as quoted by Bar-Shalom and Li [10].

Extended-Kalman-Filter-Based Seeker Estimator

Different Direction Cosine Matrices Used in Seeker

Different frames of reference used are inertial, launch local vertical (LV), pursuer body, LOS, pursuer fin, and seeker IG frame (Fig. 2) [11]. The body quaternion from LV is $\mathbf{q} = q_1 i + q_2 j + q_3 k + q_4$. Direction cosine matrix (DCM) from inertial to LV

$$C_i^{\mathrm{LV}} = \mathrm{diag}[\,1, \quad -1, \quad 1\,]$$

DCM from LV to body

$$C_{\mathrm{LV}}^b = \begin{bmatrix} q_4^2 + q_1^2 - q_2^2 - q_3^2 & 2(q_1q_2 + q_3q_4) & 2(q_1q_3 - q_2q_4) \\ 2(q_1q_2 - q_3q_4) & q_4^2 - q_1^2 + q_2^2 - q_3^2 & 2(q_2q_3 + q_1q_4) \\ 2(q_1q_3 + q_2q_4) & 2(q_2q_3 - q_1q_4) & q_4^2 - q_1^2 - q_2^2 + q_3^2 \end{bmatrix}$$

DCM from inertial to body

$$C_i^b = C_{\mathrm{LV}}^b \times C_i^{\mathrm{LV}}$$

DCM from body to fin

$$C_b^f = \begin{bmatrix} 1 & 0 & 0 \\ 0 & \frac{1}{\sqrt{2}} & \frac{1}{\sqrt{2}} \\ 0 & -\frac{1}{\sqrt{2}} & \frac{1}{\sqrt{2}} \end{bmatrix} \tag{4}$$

DCM from inertial to LOS

$$C_i^{\mathrm{LOS}} = \begin{bmatrix} \cos\gamma_l \cos\phi_l & \cos\gamma_l \sin\phi_l & \sin\gamma_l \\ -\sin\phi_l & \cos\phi_l & 0 \\ -\sin\gamma_l \cos\phi_l & -\sin\gamma_l \sin\phi_l & \cos\gamma_l \end{bmatrix}$$

In the present seeker hardware, measurements of gimbal angles (ϕ_g, γ_g) and LOS rates $(\omega_{gy}, \omega_{gz})$ are available in the IG with respect to fin frame (Fig. 2). The corresponding direction cosine (l, m, n) is

$$(l, m, n) = C_b^f C_i^b C_{\mathrm{LOS}}^i [\,1 \quad 0 \quad 0\,]^T \tag{5}$$

The gimbal angles (ϕ_g, γ_g) with respect to fin frame are

$$\phi_g = \tan^{-1}\left(\frac{m}{l}\right); \qquad \gamma_g = \tan^{-1}\left(\frac{n}{\sqrt{l^2 + m^2}}\right) \tag{6}$$

Here, the rotation sequence is

$$(\,x_f \quad y_f \quad z_f\,) \xrightarrow{\phi_g} (\,x_1 \quad y_g \quad z_f\,) \xrightarrow{-\gamma_g} (\,x_g \quad y_g \quad z_g\,)$$

and the DCM from fin to inner gimbal is

$$C_f^g = \begin{bmatrix} \cos\gamma_g \cos\phi_g & \cos\gamma_g \sin\phi_g & \sin\gamma_g \\ -\sin\phi_g & \cos\phi_g & 0 \\ -\sin\gamma_g \cos\phi_g & -\sin\gamma_g \sin\phi_g & \cos\gamma_g \end{bmatrix} \tag{7}$$

Seeker Extended Kalman Filter World Model

The state and measurement equations in the CP frame were first evolved by Ananthasayanam et al. [2,3] for seeker estimator design in open loop and are given as follows.

State Equations

The state equations are

$$\begin{aligned} \Delta\dot{x} &= \Delta V_x; \qquad \Delta\dot{y} = \Delta V_y; \qquad \Delta\dot{z} = \Delta V_z \\ \Delta\dot{V}_x &= a_{tx} - a_{mx} + w_{a_{mx}}; \qquad \Delta\dot{V}_y = a_{ty} - a_{my} + w_{a_{my}} \\ \Delta\dot{V}_z &= a_{tz} - a_{mz} + w_{a_{mz}}; \qquad \dot{a}_{tx} = -\frac{a_{tx}}{\tau_x} + w_{a_{tx}} \\ \dot{a}_{ty} &= -\frac{a_{ty}}{\tau_y} + w_{a_{ty}}; \qquad \dot{a}_{tz} = -\frac{a_{tz}}{\tau_z} + w_{a_{tz}} \end{aligned} \tag{8}$$

The evader acceleration components are modeled as first-order Gauss Markov with correlation time constant (τ_x, τ_y, τ_z).

Measurement Equations

From the state variables, the measurement equations in the IG frame are generated through the LOS frame. Interim variables along the LOS frame (Fig. 5) as a function of states are

$$\begin{aligned} \Delta x &= x_t - x_m; \qquad \Delta y = y_t - y_m; \qquad \Delta z = z_t - z_m \\ \Delta\dot{x} &= V_{tx} - V_{mx}; \qquad \Delta\dot{y} = V_{ty} - V_{my}; \qquad \Delta\dot{z} = V_{tz} - V_{mz} \\ r_l &= \sqrt{\Delta x^2 + \Delta y^2 + \Delta z^2}; \qquad \dot{r}_l = \frac{\Delta x\Delta\dot{x} + \Delta y\Delta\dot{y} + \Delta z\Delta\dot{z}}{\sqrt{\Delta x^2 + \Delta y^2 + \Delta z^2}} \\ \phi_l &= \tan^{-1}\frac{\Delta y}{\Delta x}; \qquad \dot{\phi}_l = \frac{(\Delta x\dot{\Delta y} - \Delta y\dot{\Delta x})}{(\Delta x^2 + \Delta y^2)} \\ \gamma_l &= \tan^{-1}\frac{\Delta z}{\sqrt{\Delta x^2 + \Delta y^2}} \\ \dot{\gamma}_l &= \frac{\dot{\Delta z}(\Delta x^2 + \Delta y^2) - \Delta z(\Delta x\dot{\Delta x} + \Delta y\dot{\Delta y})}{(\Delta x^2 + \Delta y^2 + \Delta z^2)(\sqrt{\Delta x^2 + \Delta y^2})} \end{aligned} \tag{9}$$

The measured LOS rates in the IG frame are obtained from the LOS frame through the transformations (Fig. 5) using Eqs. (6), (7), and (9) as

$$\begin{bmatrix} \omega_{gx} \\ \omega_{gy} \\ \omega_{gz} \end{bmatrix} = C_f^g C_b^f C_i^b C_l^i \begin{bmatrix} \dot{\phi}_l \sin\gamma_l \\ -\dot{\gamma}_l \\ \dot{\phi}_l \cos\gamma_l \end{bmatrix} \tag{10}$$

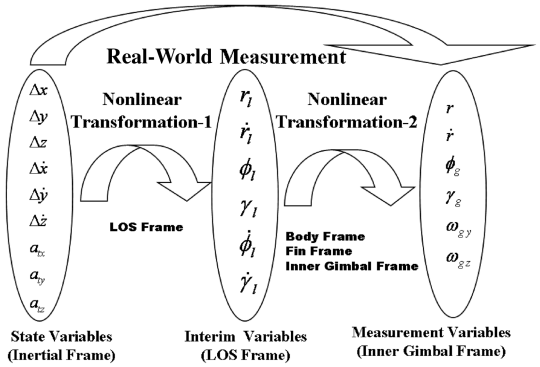

Fig. 5 State to measurements transformations.

The noisy measurements based on Eqs. (9) and (10) are

$$\begin{aligned} r_m &= r_l + \eta_1; \qquad \dot{r}_m = \dot{r}_l + \eta_2; \qquad \phi_{gm} = \phi_g + \eta_3 \\ \gamma_{gm} &= \gamma_g + \eta_4; \qquad \omega_{gym} = \omega_{gy} + \eta_5; \qquad \omega_{gzm} = \omega_{gz} + \eta_6 \end{aligned} \tag{11}$$

In Eq. (11), measurement noises $(\eta_1, \ldots, \eta_6)$ in the filter world model are modeled as Gaussian white. But in Eq. (A6) (seeker model of the Appendix), the gimbal angles and LOS rates measurements with correlated noise are generated, which mimics the real world. Now, the estimation problem consists of nine state variables of Eq. (8) and six measurements $(r_m, \dot{r}_m, \phi_{gm}, \gamma_{gm}, \omega_{gym}, \omega_{gzm})^T$ of Eq. (11). During eclipsing, four measurements $(r_m, \dot{r}_m, \phi_{gm}, \gamma_{gm})^T$ are available. Because of variable measurements over time, an estimator mechanization with sequential update [12] has been used. The inputs to the state and measurement equations are pursuer acceleration components (a_{mx}, a_{my}, a_{mz}) and its attitude quaternion **q** available from the inertial navigation system (INS). Filter tuning has been carried out based on engineering judgment similar to the radar estimator discussed earlier. In the present case, at the filter start, the LOS rate tracking error is more because of high noise. So, a smaller value of $\mathbf{P}_0 = 1E02 \times I$ has been chosen to avoid fluctuating initial transients. For **Q** tuning, $(\sigma_{a_{tx}}, \sigma_{a_{ty}}, \sigma_{a_{tz}}) = (100, 100, 100)$ m/s^2 and $(\tau_x, \tau_y, \tau_z) = (1, 1, 1)$ s have been found to be adequate. It is to be noted that process noise covariance $Q_{a_{tx}} = 2\sigma_{a_{tx}}^2/\tau_x$, and the same has been used for all acceleration channels in Eq. (8). A rule of thumb developed to calculate **R**-matrix elements, which works in all cases, is by measuring maximum random fluctuation of signal (3σ) over its mean. So, measurement variance of the ith channel is $r_{ii} = (\Delta y_i/3)^2$, where Δy_i is the maximum dispersion of the noise over the mean. Thus, the corresponding **R** matrix is

$$\text{diag}\,[2500\,\text{m}^2, 600\,\text{m/s}^2, 1\,\text{deg/s}^2, 1\,\text{deg/s}^2, r_{55i}\,\text{deg/s}^2, r_{66i}\,\text{deg/s}^2]$$

As LOS rate noise varies with instantaneous to initial range to go [Eq. (A5)], at time t_i, $r_{55i} = r_{550} \times (r_i/r_0)^4$. Here, (r_{550}, r_0) are pitch LOS rate noise covariance and range to go at seeker lock on. Similar logic is valid for the yaw channel also. Next, the CP frame estimator initialization will be discussed.

Table 1 Monte Carlo simulation [a] with Q-matrix sensitivity on radar and seeker EKF

Q factor	t_{flight}, s	Miss distance, m		Pursuer, M_{impact}
		Estimated	True	
Radar EKF (guidance, estimator) update=(20, 100) ms				
0.5	12.4 ± 0.18	35 ± 11	77 ± 13	1.45 ± 0.06
1.0	12.0 ± 0.19	25 ± 13	39 ± 17	1.58 ± 0.07
5.0	11.9 ± 0.20	31 ± 15	37 ± 20	1.60 ± 0.07
Seeker EKF (guidance, estimator) update=(10, 10) ms				
0.1	12.1 ± 0.10	22 ± 8	36 ± 12	1.65 ± 0.04
1.0	12.1 ± 0.10	8 ± 5	9 ± 6	1.67 ± 0.05
10.0	11.9 ± 0.10	9 ± 3	11 ± 4	1.63 ± 0.05

[a]MC results are normally distributed with $\mu \pm \sigma$.

Table 2 Monte Carlo simulation [a] of radar and seeker EKF with nominal Q matrix

Case type [b]	Update, ms [c]	t_{flight}, s	Miss distance, m		Pursuer, M_{impact}
			Estimated	True	
Radar, NN	10, 10	12 ± 0.1	1 ± 0.2	1 ± 0.2	1.7 ± 0.04
Radar, N	10, 10	12 ± 0.2	9 ± 4	12 ± 7	1.6 ± 0.05
Radar, N	10, 20	12 ± 0.2	13 ± 6	17 ± 9	1.6 ± 0.06
Radar, N	10, 100	15 ± 0.2	25 ± 13	39 ± 17	1.6 ± 0.7
Seeker, NN	10, 10	12 ± 0.2	1 ± 0.6	1 ± 0.6	1.7 ± 0.04
Seeker, N	10, 10	12 ± 0.1	8 ± 5	9 ± 6	1.7 ± 0.05

[a]Monte Carlo results are normally distributed with $\mu \pm \sigma$.
[b]NN = no noise, N = noise.
[c]Guidance, estimator update in milliseconds.

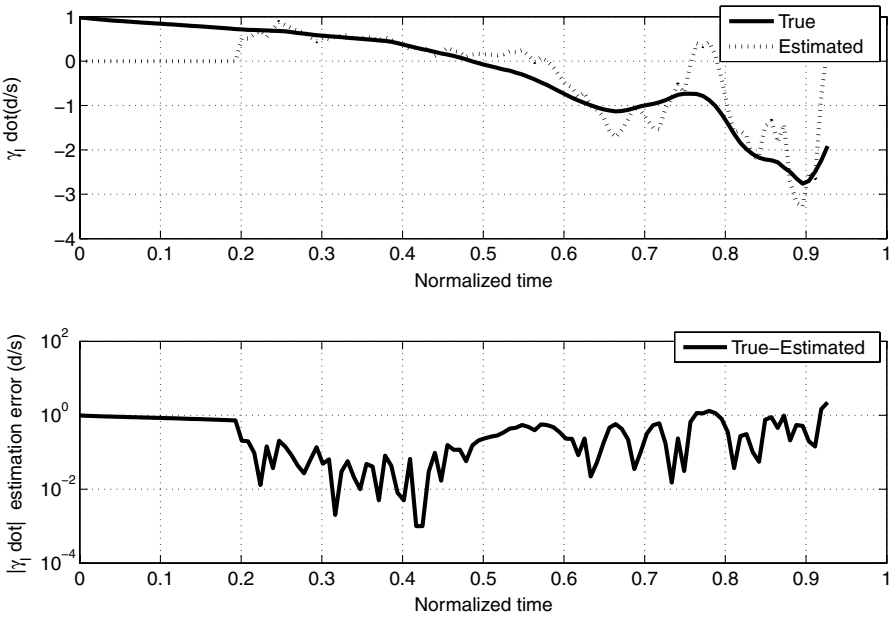

Fig. 6 Pursuer (estimated, true) pitch plane LOS rate and estimation error (100 ms radar EKF update).

The seeker EKF initialization is similar to that of the radar EKF. For this purpose, the relative position and velocity components in the C frame are calculated using Eq. (12) from the first two measurements in the IG frame using the following equation [4]:

$$\begin{bmatrix}\Delta x\\ \Delta y\\ \Delta z\end{bmatrix} = (C_i^g)^T \begin{bmatrix} r\\ 0\\ 0\end{bmatrix}; \qquad \begin{bmatrix}\Delta V_x\\ \Delta V_y\\ \Delta V_z\end{bmatrix} = (C_i^g)^T \begin{bmatrix} \dot{r}\\ r\omega_{gz}\\ -r\omega_{gy}\end{bmatrix} \tag{12}$$

Simulation Results

Both the radar and seeker estimators along with TPN guidance have been used in the 6-DOF simulation model of pursuer–evader engagement (Figs. 3 and 4). The control algorithm generates fin deflections through actuators for tracking guidance demanded latax. The actuator hardware has been modeled as a second-order system with a damping ratio of 0.36 and 20 Hz bandwidth along with a dead zone and backlash half-width of 0.23 and 0.115 deg. Based on other subsystem constraints, radar measurements and guidance update are available at 100 and 10 ms. Similarly, seeker measurements and corresponding guidance update are available in 10 ms. Hardware constraints addressed in seeker estimator design are 1) unambiguous relative range measurement update from 5 km range to go onward, and 2) guidance command generation from seeker blind zone of 100 m range to go until interception using propagated states.

A complete 6-DOF MC simulation with 200 runs of the given engagement condition has been carried out to study the robustness of filter tuning parameters. The variation in initial kinematic conditions, mass, center of gravity, moment of inertia, and thrust duration has been considered to follow a uniform distribution. The variation in different misalignment angles and aerodynamic characteristics has been considered to obey a normal distribution within specified mean and 3σ bound. The parameters of different distributions are based on experiments, wind-tunnel tests, and engineering judgment. At first, sensitivity study of $\mathbf{Q}$ matrix of both radar and seeker EKF is studied (Table 1). From Table 1, it is seen that, for lower $\mathbf{Q}$, both estimated and true miss distance is less than those corresponding to nominal $\mathbf{Q}$ values. This is because, due to low $\mathbf{Q}$, the estimated states will follow the filter model, giving rise to more tracking error and more miss

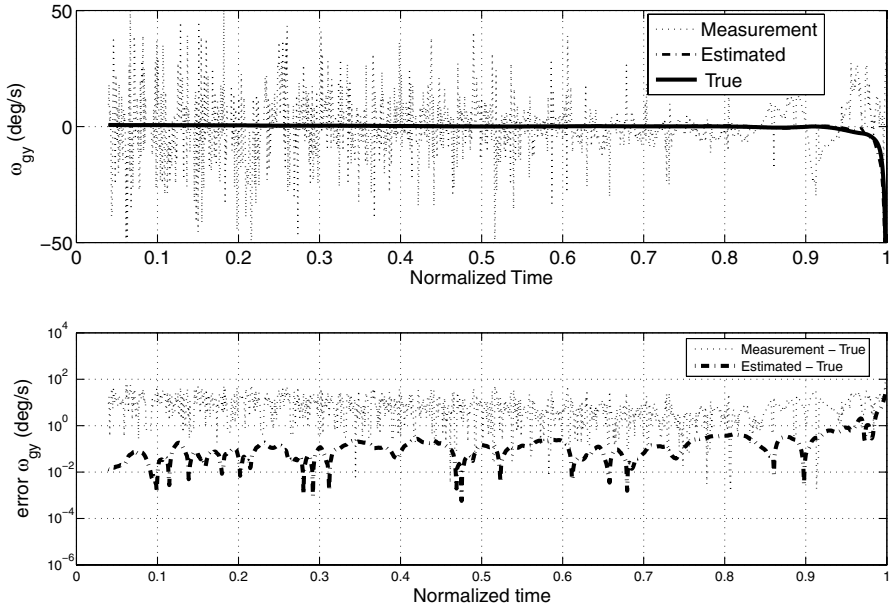

Fig. 7 Pursuer (measured, estimated, true) pitch plane LOS rate and estimation error (10 ms seeker EKF update).

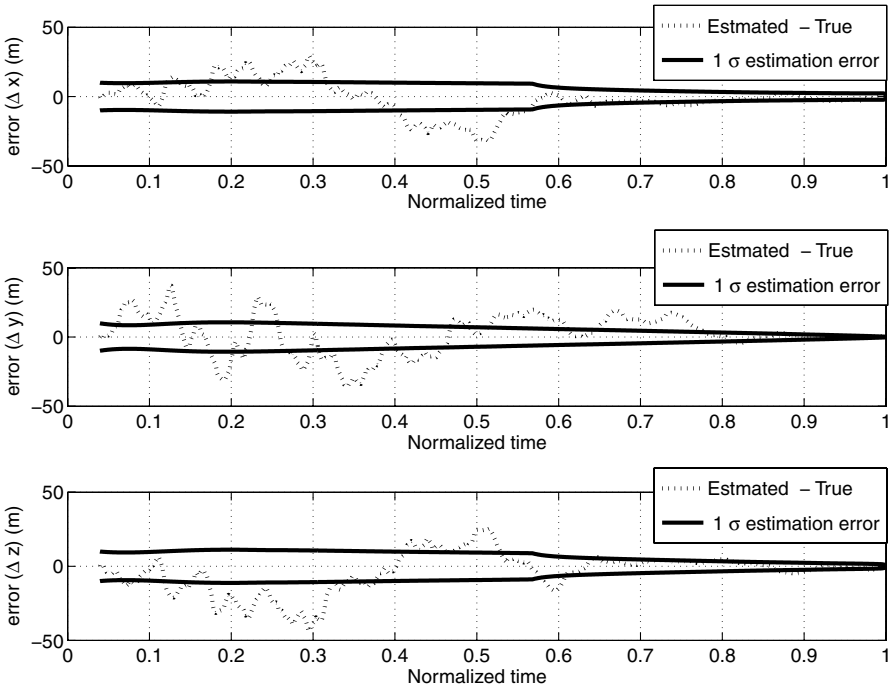

Fig. 8 Relative position estimation error (10 ms seeker EKF update).

distance. However, higher **Q** over nominal corresponds to high bandwidth filter and estimated states will tend to follow measurements. So, demanded latax will also be more noisy, which is not preferred from an actuator performance point of view. This is how a nominal balanced choice of **Q**-matrix elements corresponding to both the cases has evolved. Now, the performance of both radar and seeker estimator with nominal **Q** matrix will be discussed (Table 2). From the table, it is clear that, for the no-noise case, measurements processed at 10 ms and guidance update at 10 ms for both radar and seeker guidance give identical terminal conditions including low miss distance. Such a consistency gives confidence in the numerical adequacy of the present simulation model. But with noise, the miss distance of the radar estimator is naturally more. The lower the update rate of the radar estimator, the larger is the miss distance. For radar-based guidance with 100 ms measurement update, the time history of estimated and true pitch LOS rate and estimation error in the LOS frame is as shown in Fig. 6. The same in the IG frame for seeker-based guidance with 10 ms measurement update is shown in Fig. 7. From the figure, it is clear that, initially at higher range to go, LOS rate noise is high which is on the order of ε_p multiplied by K_v of track loop. It gradually decreases with time to go and, just before interception, it becomes high due to glint and RCS fluctuation. For more clarity, the LOS rate estimation error for both cases is shown in log scale. Relative position estimation errors in inertial frame along with (1σ) estimation accuracy are shown in Fig. 8. Initially, (1σ) estimation error is constant until 5 km range to go because of nonavailability of the range measurements. After that, the available range measurement is used for estimator update. In all figures, time

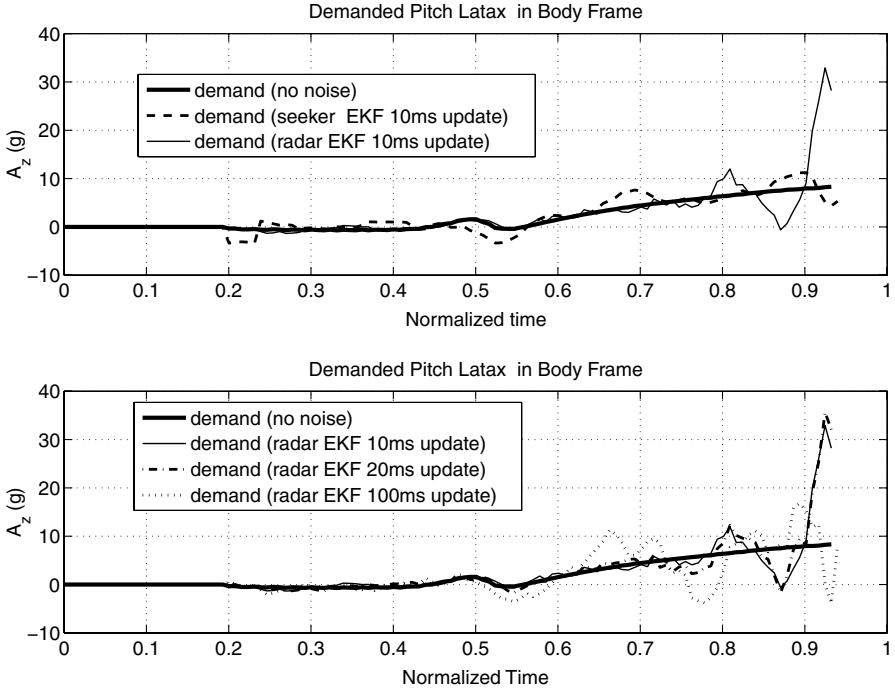

Fig. 9 Guidance demanded pitch latax (no noise, 10 ms seeker EKF update, (10, 20, 100) ms radar EKF update).

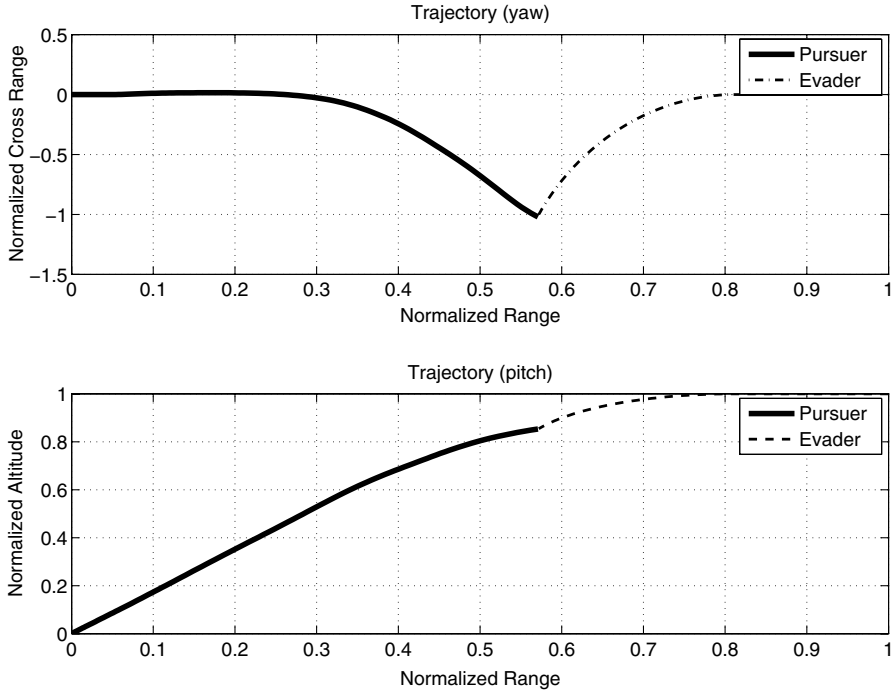

Fig. 10 Pursuer–evader trajectory.

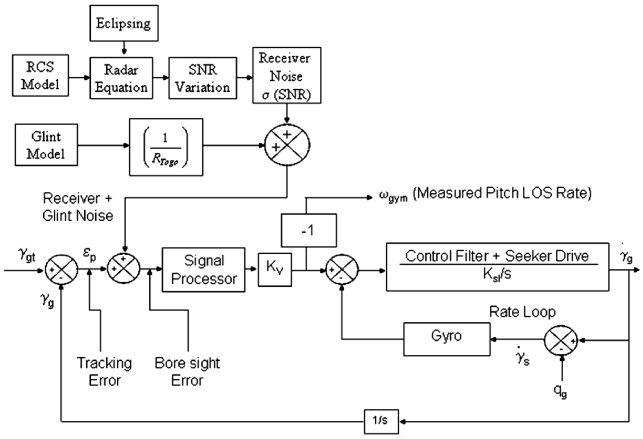

Fig. 11 Generation of pitch LOS rate in IG frame.

history has been normalized with respect to pursuer maximum flight time. By studying these figures, we infer that the tracking performance in radar-based guidance becomes oscillatory toward the endgame and the same is much better in seeker-based guidance. The reasons can be attributed as follows.

In the radar estimator, the measurement noise remains the same, independent of range to go, and the estimated states of the evader are up linked to the pursuer. Based on both evader and pursuer kinematic information, relative kinematic states are generated. Toward the endgame, when the relative position and velocity component values become on the order of the estimation error, the LOS rates will become oscillatory. But, seeker estimator relative kinematics are estimated directly from measurements and noise in the LOS rate measurement reduces with range to go, and thus toward the endgame, the oscillations in LOS rates are comparatively less. If the radar estimator update frequency is increased, namely (10, 20) ms, for tracking a maneuvering evader where the true LOS rate becomes high toward the endgame, estimation error will be less, resulting in

Table 3 Comparison of radar, seeker-based guidance

No.	Aspect	Radar	Seeker
1	Available measurements	Evader range, azimuth, elevation, and at times Doppler range rate; observability is less	Pursuer–evader relative range, range rate, gimbal angles, and LOS rates in inner gimbal frame; observability is more
2	Character of measurement noise	Can be generally assumed white Gaussian	Gimbal angles, LOS rates non-Gaussian and time correlated; LOS rates are with variable SNR as function of range to go with eclipsing, RCS, and glint noise
3	Estimator design	Simple	Relatively more complex due to correlated measurement noise
4	Measurement rate and accuracy	At 10 Hz and less accurate	At 100 Hz and more accurate
5	Demanded latax rise during endgame	Steep and oscillatory due to the noise being present during entire engagement	Small and low but cannot be fully nulled
6	Demanded latex due to autopilot, airframe limits	Limited	Not limited
7	Effect of aerodynamics	Nonlinear aerodynamics leads to poor tracking	Leads to better tracking
8	Estimation error and performance toward endgame	Position and velocity error are of same order as the measurement; performance deteriorates but blind zone cannot occur	Becomes smaller due to reduced measurement noise; performance can deteriorate during blind zone
9	Cost effectiveness and weapon characteristics	Increases but weapon system is nonautonomous	Decreases but weapon system is autonomous
10	Available literature	Plenty	Scanty

reduced oscillations in the estimated LOS rate. This, in turn, will reduce the oscillations in demanded latax and the autopilot tracking performance will be better. This improves the miss distance performance as shown in Table 2. The latax demanded by guidance along the pitch plane corresponding to all the cases of Table 2 are shown in Fig. 9. In Fig. 9, latax profiles corresponding to radar- and seeker-based guidance with 10 ms update are compared with the same corresponding to the no-noise case. Miss distance corresponding to radar guidance is more than the seeker-based guidance in the presence of noise. This is due to oscillatory latax in radar-based guidance over seeker-based guidance toward the endgame. But latax demand in seeker-based guidance is more than radar guidance at the beginning of engagement. This is because, in the seeker, the noise intensity is more as the range to go is large. So, for the same attenuation level seeker LOS rate tracking error is more, which gives to high latax demand. But in radar guidance, the noise level being constant, this situation does not arise. In the same figure, pitch latax profiles corresponding to radar-based guidance with (10, 20, 100) ms update are compared with the same corresponding to the no-noise case. As explained earlier for lower measurement update rate, higher is the LOS rate tracking error, as well as oscillations in demanded latax toward the endgame while tracking a maneuvering evader. This gives rise to increased autopilot tracking error due to nonlinear aerodynamics and higher miss distance (Table 2). Figure 10 shows the azimuth and elevation trajectories corresponding to a typical pursuer–evader engagement considered here. Pure planar pitch or yaw-only engagement studies in the simulations also provide similar conclusions.

Conclusions

In the present investigation, a performance comparison of radar- and seeker-based guidance (Table 3) for intercepting a maneuvering evader through a realistic 6-DOF simulation of a surface-to-air engagement has been carried out. A hardware-driven novel seeker estimator formulation, track-loop model for generating gimbal angles and LOS rate measurements in the IG frame contaminated by time correlated noise have been discussed. Also, the noise components in LOS rates vary from low to high SNR from initial range to go until interception. A pursuer OBC implementable TPN guidance algorithm has also been discussed herein. The present seeker estimator is based on a standard EKF in CP frame, and a more appropriate glint noise modeling [13] along with interacting multiple models [10] features could provide improved state estimates in the future. This work is also being extended for using the radar estimator for midcourse and seeker estimator for terminal application. Numerical linearization of nonlinear measurement equations has to be carried out analytically for real-time application. Possible extension of present seeker estimator in the CP frame to the PPG frame with adaptive filter tuning and their performance comparison [14] is an open area of future research.

Appendix: Some Modeling Aspects of the Scenario and Guidance Formulations

Evader Modeling

A three dimensional evader kinematic point mass model is available in [11]. The pursuer being airbreathing, forward speed is assumed constant and latax is pulled along the yaw and pitch planes.

Seeker Track-Loop Model

In an actual seeker, the LOS rates $(\omega_{gy}, \omega_{gz})$ in the IG frame (Fig. 2) are generated from gimbal angles' (γ_g, ϕ_g) tracking error in the presence of body rate coupling. The schematic diagram of generating ω_{gy} in the IG frame is shown in Fig. 11 based on Ekstrand's formulation [4]. In the present hardware, INS sensed body rates (p, q, r) in the body frame are transformed to fin and IG frame as

$$\begin{bmatrix} p_f \\ q_f \\ r_f \end{bmatrix} = C_b^f \begin{bmatrix} p \\ q \\ r \end{bmatrix}; \qquad \begin{bmatrix} p_g \\ q_g \\ r_g \end{bmatrix} = C_f^g C_b^f \begin{bmatrix} p \\ q \\ r \end{bmatrix} \tag{A1}$$

$$\begin{bmatrix} \omega_{gx} \\ \omega_{gy} \\ \omega_{gz} \end{bmatrix} = \begin{bmatrix} \dot{\phi}_g \sin\gamma_g \\ -\dot{\gamma}_g \\ \dot{\phi}_g \cos\gamma_g \end{bmatrix} + \begin{bmatrix} p_g \\ q_g \\ r_g \end{bmatrix} \tag{A2}$$

From Eq. (A2) the LOS rates in the IG frame are

$$\begin{bmatrix} \omega_{gy} \\ \omega_{gz} \end{bmatrix} = \begin{bmatrix} (\dot{\gamma}_g - q_g) & \times & (-1) \\ (\dot{\phi}_g + \frac{r_g}{\cos\gamma_g}) & \times & (\cos\gamma_g) \end{bmatrix} \tag{A3}$$

The track-loop block diagram (Fig. 2) corresponds to the generation of ω_{gy} where K_{sl} is the seeker stabilization loop gain. Yaw plane characteristics are similar.

Real-World Seeker Measurements

The angle tracking noise is modeled as a Gaussian with standard deviation σ_m. This standard deviation of angle tracking noise is related to the receiver SNR as $\sigma_m = K_1/\sqrt{\text{SNR}}$. Again, $\text{SNR} = (Kdr^2)/R_{\text{to-go}}^4$ where $dr = \tau_R/T_p$ is a cyclic time-varying quantity varying between 0 and $\varepsilon_{\max}$ due to eclipsing, where $\varepsilon_{\max}$ depends on the receiver gate mechanism of a particular seeker. For the no-eclipsing case, dr can be taken as $\varepsilon_{\max}$. Again, combining the preceding equations,

$$\sigma_m = (K_1/\sqrt{K})(r_{\text{to-go}}^2/dr) = K_2(r_{\text{to-go}}^2/dr) \tag{A4}$$

If $\sigma_m = \sigma_{\max}^o$ at $r_{\max}$ km, $K_2 = \varepsilon_{\max}(\sigma_{\max}/r_{\max})^2$. For any $r_{\text{to-go}}$, angle tracking noise is expressed as

$$\sigma = \sigma_{\max}(r_{\text{to-go}}/r_{\max})^2(\varepsilon_{\max}/dr) \tag{A5}$$

The true angle tracking errors $(\varepsilon_y, \varepsilon_p)$ are contaminated by receiver noise and glint noise (w_p, w_y) [15]. The thermal noise $(\sigma_{\phi_g}, \sigma_{\gamma_g})$ is assumed to obey a normal distribution. So, the seeker measurement equations in the gimbal frame are (Fig. 11)

$$\begin{aligned} r_m &= r_l + \eta_1; \qquad \dot{r}_m = \dot{r}_l + \eta_2 \\ \phi_{gm} &= \frac{\{K_{\text{sl}}[K_v\phi_{gt} - (r_g/\cos\gamma_g)] + K_{\text{sl}}K_v w_y\}}{s^2 + K_{\text{sl}}s + K_{\text{sl}}K_v} + \mathcal{N}(0, \sigma_{\phi_g}) \\ \gamma_{gm} &= \frac{\{K_{\text{sl}}(K_v\gamma_{gt} + q_g) + K_{\text{sl}}K_v w_p\}}{s^2 + K_{\text{sl}}s + K_{\text{sl}}K_v} + \mathcal{N}(0, \sigma_{\gamma_g}) \\ \omega_{gym} &= -(\varepsilon_p + w_p)K_v; \qquad \omega_{gzm} = (\varepsilon_y + w_y)K_v\cos\gamma_g \end{aligned} \tag{A6}$$

Here (η_1, η_2) are zero mean Gaussian noise. Before the gimbal angle, receiver noise components appear as filtered noise throughout track-loop lag s/K_v. The gimbal angle is a slowly varying process contaminated by track-loop lag filter receiver noise and Gaussian measurement noise $(\sigma_{\phi_g}, \sigma_{\gamma_g})$. It is to be noted that $(\omega_{gy}, \omega_{gz})$ are obtained from Eq. (A3), which includes the effect of body motion coupling and it is contaminated by correlated noise in Eq. (A6). At every sampling time, true $(r, \dot{r}, \phi_g, \gamma_g, \omega_{gy}, \omega_{gz})$ are contaminated by seeker noise based on the methodology given previously and are used as measurements. The hardware-compatible noise figures of different channels are now given. The noise level of η_1 is $\mathcal{N}(0, 50)$ m and that of η_2 is $\mathcal{N}(0, 25)$ m/s. The same for $(\varepsilon_p, \varepsilon_y)$ are $\mathcal{N}(0, 1.0)$ deg, respectively. The thermal noise $(\sigma_{\phi_g}, \sigma_{\gamma_g})$ is based on $\mathcal{N}(0, 2)$ deg. Based on the preceding equation, the noise in $(\omega_{gym}, \omega_{gzm})$ are $[(\varepsilon_p + w_p)K_v,\ (\varepsilon_y + w_y)K_v\cos\gamma_g]$. The track-loop gains $(K_{\text{sl}}, K_v) = (300, 10)$.

True Proportional Navigation Formulation for Radar-Based Guidance

The estimated evader position and velocity information are uplinked to the pursuer through a data link. If not available, these are extrapolated from the previous instant as

$$x_{t,i+1} = x_{t,i} + \dot{x}_{t,i}\Delta t; \qquad y_{t,i+1} = y_{t,i} + \dot{y}_{t,i}\Delta t$$
$$z_{t,i+1} = z_{t,i} + \dot{z}_{t,i}\Delta t; \qquad \dot{x}_{t,i+1} = \dot{x}_{t,i}; \qquad \dot{y}_{t,i+1} = \dot{y}_{t,i}$$
$$\dot{z}_{t,i+1} = \dot{z}_{t,i} \tag{A7}$$

Using the pursuer position, velocity from INS and the estimated evader states $(r, \dot{r}, \phi_l, \gamma_l, \dot{\phi}_l, \dot{\gamma}_l)$ are calculated based on Eq. (9). Based on these, the demanded latax along LOS are computed and transferred to the body as [16]

$$\begin{bmatrix} a_{xd} \\ a_{yd} \\ a_{zd} \end{bmatrix}_b = NC_{\mathrm{LV}}^b C_i^{\mathrm{LV}} C_{\mathrm{LOS}}^i \begin{bmatrix} 0 \\ V_c\dot{\phi}_l \cos\gamma_l \\ V_c\dot{\gamma}_l \end{bmatrix}_{\mathrm{LOS}} \tag{A8}$$

The closing velocity $V_c = -\dot{r}$. A modified PN [17] based on forward acceleration compensation along the body frame is used in pursuer OBC for achieving better miss distance in practice, which is discussed now. According to the TPN from Eq. (A8),

$$\begin{bmatrix} a_{xm} \\ a_{ybd} \\ a_{zbd} \end{bmatrix}_b = \begin{bmatrix} c_{11} & c_{12} & c_{13} \\ c_{21} & c_{22} & c_{23} \\ c_{31} & c_{32} & c_{33} \end{bmatrix} \begin{bmatrix} a_{xd} \\ a_{yd} \\ a_{zd} \end{bmatrix}_{\mathrm{LOS}} \tag{A9}$$

where $\mathbf{a}_m = [a_{xm}, a_{ybd}, a_{zbd}]^T$ is the pursuer total acceleration including latax a_{ybd}, a_{zbd}, and forward acceleration a_{xm} along the body frame. The demanded latax along the LOS frame being $\mathbf{a}_d = [a_{xd}, a_{yd}, a_{zd}]^T$, using Eq. (A9):

$$a_{xd} = [a_{xm} - (c_{12}a_{yd} + c_{13}a_{zd})]/c_{11} \tag{A10}$$

The acceleration component a_{xd} in Eq. (A10) is the compensated acceleration term obtained from longitudinal acceleration available from INS. Now, $[\mathbf{a}_d]_{\mathrm{LOS}}^{\mathrm{modified}} = (a_{xd}, a_{yd}, a_{zd})$ are demanded latax in the LOS frame and transformed to the body frame using Eq. (A9) as

$$\mathbf{a}_m^b = (a_{xdm}, a_{ydm}, a_{zdm}) = C_{\mathrm{LV}}^b C_i^{\mathrm{LV}} C_{\mathrm{LOS}}^i [\mathbf{a}_d]_{\mathrm{LOS}}^{\mathrm{modified}} \tag{A11}$$

The latax components (a_{ydm}, a_{zdm}) of Eq. (A11) are tracked by autopilot.

True Proportional Navigation Formulation for Seeker-Based Guidance

The seeker estimates $(r, \dot{r}, \phi_g, \gamma_g, \omega_{gy}, \omega_{gz})$ [Eq. (11)] are available in the IG frame. The closing velocity is $\mathbf{V}_g = [V_c \quad 0 \quad 0]^T$. So, the demanded pursuer latax according to TPN guidance from IG to body frame is

$$\begin{bmatrix} a_{xdm} \\ a_{ydm} \\ a_{zdm} \end{bmatrix}_b = NC_f^b C_g^f (\omega_g \times \mathbf{V}_g) = C_f^b C_g^f \begin{bmatrix} a_{xmg} \\ a_{ymg} \\ a_{zmg} \end{bmatrix}_g \tag{A12}$$

Now, the pursuer OBC implementable PN formulation compatible to Eqs. (A10) and (A11) is

$$\begin{bmatrix} a_{xdm} \\ a_{ydm} \\ a_{zdm} \end{bmatrix}_b = C_g^b \begin{bmatrix} [a_{xbm} - (c_{12}a_{ydm} + c_{13}a_{zdm})]/c_{11} \\ a_{ymg} \\ a_{zmg} \end{bmatrix}_i \tag{A13}$$

The autopilot tracks the latax components (a_{ydm}, a_{zdm}).

Acknowledgments

We thank the authorities of the Defence Research and Development Laboratory for projecting the need and giving us permission to publish the present research. We also sincerely thank the anonymous referees for their useful comments which helped to improve the presentation substantially.

References

[1] Lin, C. F., *Modern Navigation, Guidance and Control Processing*, 1st ed., Prentice–Hall, Upper Saddle River, NJ, 1991.

[2] Ananthasayanam, M. R., Sarkar, A. K., Vorha, P., Bhattacharya, A., and Srivastava, R., "Estimation of LOS Rates and Angles Using EKF from Seeker Measurements," *Proceedings of International Conference on Signal Processing and Communications*, SPCOM04, Nov. 2004, http://ieeexplore.ieee.org/stamp/stamp.jsp?tp=&arnumber=1458515&isnumber=31229.

[3] Ananthasayanam, M. R., Sarkar, A. K., Bhattacharya, A., Tiwari, P., and Vorha, P., "Nonlinear Observer State Estimation from Seeker Measurements and Seeker-Radar Measurements Fusion," AIAA Paper No. 2005-6066-CP, Aug. 2005.

[4] Ekstrand, B., "Tracking Filters and Models for Seeker Applications," *IEEE Transactions on Aerospace and Electronic Systems*, Vol. 37, No. 3, July 2001, pp. 965–977. doi:10.1109/7.953250

[5] Zarchan, P., *Tactical and Strategic Missile Guidance*, 4th ed., AIAA, Reston, VA, 2002.

[6] Chen, R. H., Speyer, J. L., and Lianos, D., "Homing Missile Guidance and Estimation Under Agile Target Acceleration," *Journal of Guidance, Control, and Dynamics*, Vol. 30, No. 6, Nov. 2007, pp. 1577–1589. doi:10.2514/1.30107

[7] Vaddi, S. S., Menon, P. K., and Ohlmeyer, E. J., "Target State Estimation for Integrated Guidance-Control of Missiles," AIAA Paper No. 2007-6838-CP, Aug. 2007.

[8] Kaplan, J. A., "The Analysis of a Generic Air to Air Missile Simulation Model," NASA TR TM 109057, June 1994.

[9] Broadston, R. D., Hutchins, R. G., Titus, H. A., and Swee, C. S., "Hybrid Guidance Laws for Improved Missile Intercept Range," AIAA Paper No. 2002-4654-CP, Aug. 2002.

[10] Bar-Shalom, Y., and Li, X. R., *Estimation and Tracking, Principles, Techniques and Software*, 1st ed., Artech House, Boston, 1993.

[11] Siouris, G. M., *Missile Guidance and Control*, 1st ed., Springer–Verlag, Berlin, 2004.

[12] Stengel, R., *Stochastic Optimal Control with Theory and Applications*, 1st ed., Wiley, New York, 1986.

[13] Wu, W. R., "Target Tracking with Glint Noise," *IEEE Transactions on Aerospace and Electronic Systems*, Vol. 29, No. 1, Jan. 1993, pp. 174–185. doi:10.1109/7.249123

[14] Balakrishnan, S. N., "Extension to Modified Polar Coordinates and Applications with Passive Measurements," *Journal of Guidance, Control, and Dynamics*, Vol. 12, No. 6, Dec. 1989, pp. 906–912. doi:10.2514/3.20499

[15] Borden, B. H., and Mumford, M. L., "A Statistical Glint/Radar Cross Section Evader Model," *IEEE Transactions on Aerospace and Electronic Systems*, Vol. 19, No. 5, Sept. 1983, pp. 781–785. doi:10.1109/TAES.1983.309383

[16] Hablani, H. B., "Gaussian Second Order Filter for Proportional Navigation of Exoatmosphere Interceptors with Angle Only Measurements," AIAA Paper No. 98-4217-CP, Aug. 1998.

[17] Sarkar, A. K., Tiwari, P. K., Srinivasan, S., Bhattacharjee, R. N., and Ghose, D., "Generalized PN Guidance Law for a Practical Pursuer Evader Engagement," AIAA Paper No. 2003-5651-CP, Aug. 2003.